analytical chemistry

Article

pubs.acs.org/ac

"From the Edge to the Center": Viscoelastic Migration of Particles and Cells in a Strongly Shear-Thinning Liquid Flowing in a Microchannel

Francesco Del Giudice,*[,†,¶] Shivani Sathish,[†] Gaetano D'Avino,[‡] and Amy Q. Shen*[,†]

[†]Micro/Bio/Nanofluidics Unit, Okinawa Institute of Science and Technology Graduate University, 1919-1 Tancha, Onna-son, Kunigami-gun, Okinawa 904-0495, Japan

[‡]Dipartimento di Ingegneria Chimica, dei Materiali e della Produzione Industriale, Universitá degli Studi di Napoli Federico II, Piazzale Tecchio 80, 80125 Naples, Italy

[¶]Systems and Process Engineering Centre, College of Engineering, Swansea University, Fabian Way, Swansea SA1 8EN, U.K.

Supporting Information

ABSTRACT: Controlling the fate of particles and cells in microfluidic devices is critical in many biomedical applications, such as particle and cell alignment and separation. Recently, viscoelastic polymer solutions have been successfully used to promote transversal migration of particles and cells toward fixed positions in straight microchannels. When inertia is negligible, numerical simulations have shown that strongly shear-thinning polymer solutions (fluids with a shear viscosity that decreases with increasing flow rates) promote transversal migration of particles and cells toward the corners or toward the centerline in a straight microchannel with a square cross section, as a function of particle size, cell deformability, and channel height. However, no experimental evidence of such shifting in the positions for particles or cells suspended in strongly shear-thinning liquids has been presented so far. In this work, we demonstrate that particle positions over the channel cross section can be shifted "from the edge to the center" in a strongly shear-thinning liquid. We investigate the viscoelasticity-induced migration of both rigid particles and living cells (Jurkat cells and NIH 3T3 fibroblasts) in an aqueous 0.8 wt % hyaluronic acid solution. The combined effect of fluid elasticity, shear-thinning, geometric confinement, and cell deformability on the distribution of the particle/cell positions over the channel cross section is presented and discussed. In the same shear-thinning liquid, separation of 10 and 20 μm particles is also achieved in a straight microchannel with an abrupt expansion. Our results envisage further applications in viscoelasticity-based microfluidics, such as deformability-based cell separation and viscoelastic spacing of particles/cells.

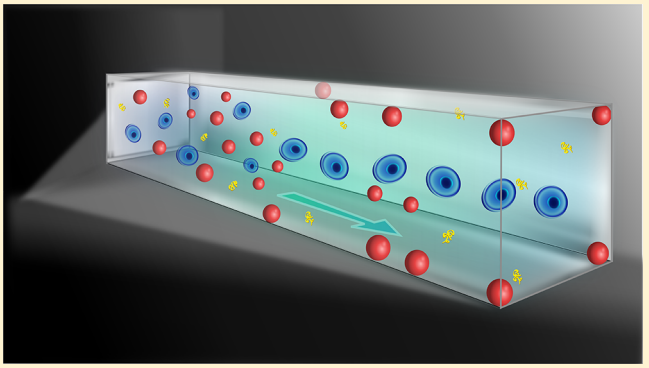

In the last decades, microfluidic platforms have been widely used to manipulate the trajectories of particles and living cells in channels with micrometer-size scale.[1−4] Microfluidic operations such as sorting, analysis, and detection require a precise control of the flowing particle trajectories. For instance, the size and the variance of a population of cells can be determined more accurately when such cells are aligned along the centerline of a microfluidic channel.[5] For biomedical applications, separation of healthy cells from unhealthy cells (such as circulating tumor cells) can be accomplished in an ad hoc microfluidic device based on the deformability difference between healthy and unhealthy cells.[6]

Several techniques have been proposed to manipulate the trajectories of particles suspended in a fluid. Many of them rely on the use of external forces generated, for instance, by electric,[7] magnetic,[8] or acoustic[9] fields. The resulting platforms are, however, sometimes bulky, and require fine-tuning of the field strength. Furthermore, particles or cells need to be functionalized to be responsive to the external field before each experiment, thus limiting rapid healthcare applications.

An alternative way to manipulate the trajectories of the flowing particles is through forces intrinsic to the suspending fluid. For instance, particles suspended in water and flowing in a microchannel migrate transversally to the flow direction if inertial forces become relevant.[10−13] The so-called inertial microfluidics have been successfully used for the alignment[14] and separation[15] of cells, avoiding any preliminary cell treatment. However, inertial effects may become weak with submicrometer-sized particles, small channel dimensions, and/or small flow rates.[16]

Recently, particle and cell manipulation has been successfully achieved in simple straight microchannels by replacing the

Received: June 23, 2017
Accepted: October 30, 2017
Published: October 30, 2017

DOI: 10.1021/acs.analchem.7b02450
Anal. Chem. 2017, 89, 13146−13159

suspending liquid from pure water to dilute aqueous polymer solutions.[16−18] The flow field developed in the channel leads to deformation of the polymer chains, resulting in a net elastic force that pushes the particles toward the channel centerline or the walls, depending on the elastic properties, i.e., the rheology of the polymer solution, and on the volumetric flow rate.[16,17] Most of the works available in the literature have considered elastic fluids with a near-constant viscosity. In this case, fluid elasticity drives the particles and cells toward the channel centerline achieving the so-called particle[19−22] or cell[23,24] focusing.

The literature dealing with particle manipulation in elastic fluids with a nonconstant viscosity is scarce. The degree of shear-thinning fluids is commonly quantified by the flow index parameter n.[25] With reference to the simple shear flow case, the shear-thinning region of the viscosity η can be related to the shear rate $\dot{\gamma}$ through a power-law model $\eta \propto \dot{\gamma}^{n-1}$, with $0 < n \leq 1$. For a constant-viscosity fluid the flow index is $n = 1$. Lindner et al.[26] proposed to classify the fluid as weakly or strongly shear-thinning if $n \geq 0.65$ or $n < 0.65$, respectively. Lim et al.[27] used an aqueous hyaluronic acid (HA) solution at 0.1 wt % ($n \approx 0.9$) to align rigid particles and white blood cells on the centerline of a rectangular microfluidic channel by coupling elastic and inertial effects. Nam et al.[28] used the same 0.1 wt % HA solution to align and separate human breast carcinoma and leukocyte cells in a straight microfluidic channel. Liu et al.[29] reported that particles, cells, and bacteria suspended in a 0.2 wt % PEO solution ($n \approx 0.8$) attained different equilibrium positions depending on their size and the aspect ratio of the channel, allowing easy separation. In square-shaped geometry, they found that 5 μm particles migrated toward the channel centerline, while 15 μm particles were off-centered with respect to the centerline. Very recently, Yuan et al.[30] used a 0.1 wt % poly(ethylene oxide) (PEO) aqueous solution ($n \approx 0.9$) to align and separate Jurkat and Yeast cells. Seo et al.[31] employed a holographic microscopy technique to study the transversal migration of rigid particles suspended in a 1 wt % PEO aqueous solution ($n \approx 0.65$). They found that the shear-thinning property promoted the depletion of some rigid particles from the centerline, leading some particles to migrate toward the centerline and others toward the vicinity of the walls. Del Giudice et al.[32] used an aqueous PEO solution at 1.6 wt % ($n = 0.5$) and observed the presence of 10 μm particles in the four corners of a straight square-shaped microfluidic channel with a channel height $H = 100$ μm, in agreement with numerical simulations.[33]

While elastic near-constant-viscosity liquids are expected to promote particle migration toward the channel centerline only, numerical simulations showed that strongly shear-thinning liquids promoted transversal migration of rigid particles and cells either toward the corners or toward the centerline of a square-shaped microchannel as a function of the particle diameter, cell deformability, channel size, and volumetric flow rate, without changing the suspending liquid.[33,34] However, no experimental evidence of such shifting in the equilibrium positions for particles and cells in strongly shear-thinning liquids, with negligible inertia, has been reported. Needless to say, a detailed investigation on the transversal migration of particles and cells in shear-thinning liquids would provide a deeper understanding of the effect of fluid rheology on the transversal migration of particles and cells. Moreover, shear-thinning liquids are expected to be more beneficial for delicate cells (such as neuron cells[35]) as compared to near constant-viscosity liquids. The velocity profile around the centerline of a straight microfluidic channel is flat (Figure 3), leading to smaller stresses on the cell surface as compared to the near constant-viscosity case, at the same volumetric flow rate. Furthermore, the viscosity thinning at high flow rates reduces the pressure drop required to pump the suspension through the microfluidic channel, reducing risks connected to high-pressure-induced device failure.

In this work, we demonstrate that positions of particles over the channel cross section can be shifted "from the edge to the center" in a strongly shear-thinning liquid flowing in a straight square-shaped microchannel, when inertia is negligible. We use polystyrene particles with four different diameters and two types of cells, namely Jurkat cells and NIH 3T3 fibroblasts with different deformabilities. The suspending liquid is an aqueous solution of hyaluronic acid at 0.8 wt % with a flow index $n = 0.35$. Optical microscopy techniques and numerical simulations are used to measure the position of the flowing particles on the channel cross section at a fixed distance from the channel inlet. The effect of flow rate, particle size, and deformability on the equilibrium positions attained by the particles and cells is presented and discussed. The present results are also compared with experimental and numerical observations available in the literature for near-constant viscosity as well as weakly and strongly shear-thinning elastic fluids. Finally, separation of 10 and 20 μm particles in HA 0.8 wt % is achieved in a straight microchannel with an abrupt expansion.

THEORETICAL BACKGROUND

Dimensionless Parameters. The interplay among different migration mechanisms can be studied by comparing the relevant transversal forces acting on particles and cells. Unfortunately, while an expression for the deformability-induced force is known,[23] an explicit expression for the migration force induced by a viscoelastic suspending fluid with shear-thinning features is not available. In this regard, it is worthwhile noting that the expressions of the viscoelastic force descriptions commonly used in the literature[17] depend on the Deborah number and the confinement ratio only, but this is valid only for constant-viscosity fluids at small Deborah numbers. These conditions are not met in our experiments. A similar expression for a general viscoelastic fluid with shear-thinning features is difficult to derive, as it needs to be valid for nonvanishing Deborah numbers (when shear-thinning effects start to become relevant), likely leading to complex and nonlinear dependences on the relevant dimensionless parameters. Alternatively, numerical simulations[33,36] can be employed to examine the particle migration behavior by elucidating the interplay among different migration mechanisms through dimensionless numbers, highlighting the importance of relevant forces.

Fluid viscoelasticity can be quantified by the Deborah number De. For square-shaped channel geometries, De is defined as

$$De = \frac{\lambda Q}{H^3} \tag{1}$$

The Deborah number is the ratio between the fluid characteristic time λ (generally the longest relaxation time) and the flow characteristic time H^3/Q, where H is the channel height, and Q is the volumetric flow rate. For a Newtonian fluid (zero elasticity), the Deborah number is $De = 0$, while larger De corresponds to more pronounced elasticity present in the fluid.

DOI: 10.1021/acs.analchem.7b02450
Anal. Chem. 2017, 89, 13146−13159

Another important dimensionless number is the Reynolds number

$$Re = \frac{\rho Q}{\eta H} \tag{2}$$

where ρ is the density, and η the shear viscosity of the liquid. Re represents the ratio between inertial and viscous forces. The highest Reynolds number for the system considered in this work is $O(10^{-3})$, thus inertial effects are insignificant.

To quantify the particle deformability, we use the elastic capillary number

$$Ca_{el} = \frac{\eta Q}{G H^3} \tag{3}$$

where G is the storage modulus of the object. Ca_{el} is the ratio between the viscous force from the suspending liquid and the elastic force from the deformable object. For a rigid particle, the elastic capillary number is $Ca_{el} = 0$.

The confinement ratio is defined as

$$\beta = \frac{d}{H} \tag{4}$$

the ratio between the particle or cell diameter d and the channel height H.

Forces Acting on Particles and Cells Suspended in Shear-Thinning Liquids. For particles and cells suspended in a near constant-viscosity liquid, the direction of the transversal migration does not depend on the Deborah number De[16,17,19,34] (or on the flow rate Q). In shear-thinning liquids,[33] instead, the migration direction is strongly dependent on De (Figure 1). Villone et al.[33] reported the existence of a neutral plane along the channel cross section, which identifies the basin of attraction for rigid particles. A rigid particle initially positioned (i.e., at the channel inlet) within the neutral plane migrates toward the channel centerline as the elastic force within the neutral plane is directed toward the centerline. On the other hand, a rigid particle with its center of gravity outside the neutral plane migrates toward the channel corners (Figure 1). The size of the neutral plane is strongly affected by the Deborah number De. Increasing the Deborah number leads to a modification of the velocity profile in the microchannel, affecting, in turn, the direction of the viscoelastic force. Specifically, higher De-values reduce the area of the neutral plane, reducing the fraction of particles focused on the centerline as well (Figure1b). Hence, most of the particles are attracted toward the centerline at low Deborah numbers and toward the corners at high Deborah numbers. Notice that a quantification of "low" and "high" Deborah number depends on the rheology of the fluid under investigation and on the confinement ratio β. To the best of our knowledge, no general criterion has been presented so far to quantitatively discriminate between "low" and "high" Deborah numbers. Very recently, Li et al.[37] have proposed a similar model for particles suspended in a weakly shear-thinning hyaluronic acid solution. The proposed model was based on decomposing the elastic force in a component directed toward the wall and another directed toward the centerline.

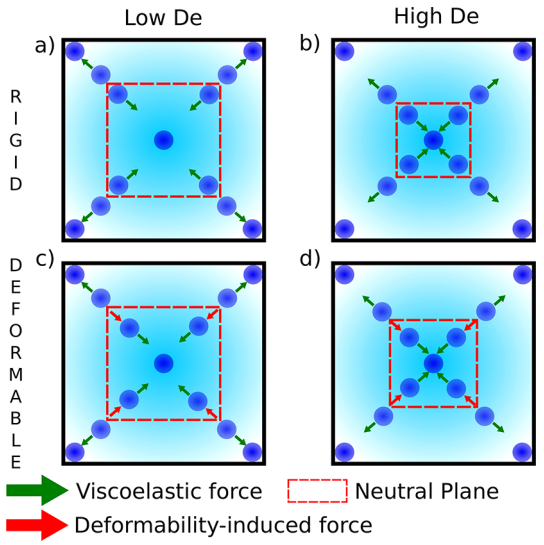

Figure 1. Rigid particles and deformable objects migrate toward different positions depending on flow conditions. Schematic of the forces acting on rigid particles and deformable objects, depending on the Deborah number $De = \lambda Q/H^3$, where λ is the fluid relaxation time, Q is the volumetric flow rate, and H is the channel height. The red dashed line is the so-called neutral plane.[33,36] If the initial position (i.e., at the channel inlet) of the object along the cross section is within the neutral plane, it migrates toward the centerline; otherwise the object migrates toward the corners. (a) Rigid particles at low De. (b) Rigid particles at high De. (c) Deformable objects at low De. (d) Deformable objects at high De.

For deformable objects (such as cells) suspended in shear-thinning liquids, a deformability-induced force directed toward the channel centerline[23] (Figure 1c,d) affects the transversal migration. In this case, the position of the neutral plane depends on the mutual strength of viscoelastic and deformability-induced force, quantified through the Deborah number De and the elastic capillary number Ca_{el}, respectively. Similar to rigid objects, deformable particles entering the channel at a position within the neutral plane migrate toward the centerline, while those outside the neutral plane migrate toward the corners (Figure 1c,d). Unfortunately, a general theory on the coupled effect of these forces on the migration is not available. Numerical simulations of Villone et al.[36] reported only a few representative cases, which are compared with our experimental observations (Transveral Migration of Cells).

The values of the dimensionless numbers for the experiments carried out in this work are listed in Table 1.

MATERIALS AND METHODS

Fluid Rheology. The suspending liquid used in this work is a 0.8 wt % aqueous solution of hyaluronic acid (HA) (molecular weight M_w = 1.6 MDa, Sigma-Aldrich, Japan). HA is a polyelectrolyte, i.e., a polymer with free charges on the chain. Because of electrostatic repulsion, free charges cause the swelling of the polymer (large hydrodynamic radius),[38,39] enhancing shear-thinning properties. HA is usually used in combination with phosphate buffer saline (PBS) to promote cell viability during and after biological experiments.[27] However, PBS contains 138 mM of NaCl, and Na^+ ions in solution screen free charges on polyelectrolyte chains, causing polymer shrinking, leading to a decrease in both shear-thinning properties and elasticity[40] (see also Figure S1). Thus, for this work, PBS is not added to the HA to preserve both shear-thinning and elastic properties.

Rheological measurements were carried out on a stress controlled rheometer (Anton Paar MCR 502) with a cone and plate geometry (50 mm of diameter, 1° angle). Solvent trap was

DOI: 10.1021/acs.analchem.7b02450
Anal. Chem. 2017, 89, 13146−13159

Table 1. Values of the Dimensionless Numbers Corresponding to the Experiments Performed in This Work[a]

	$\beta = d/H$	Q [μL/min]	$De = \lambda Q/H^3$	$Re = \rho Q/(\eta H)$	$Ca_{el} = \eta Q/(GH^3)$
			rigid particles		
polystyrene	$0.06 < \beta < 0.2$	0.1	0.92	4.3×10^{-6}	0
		0.25	2.3	1.5×10^{-5}	0
		0.5	4.6	4.2×10^{-5}	0
		1	9.2	1.2×10^{-4}	0
		2	18	3.7×10^{-4}	0
		4	37	1.1×10^{-3}	0
		8	74	3.6×10^{-3}	0
			cells		
Jurkat	$\beta = 0.14 \pm 0.02$	0.1	0.92	4.3×10^{-6}	0.13
		0.25	2.3	1.5×10^{-5}	0.24
		0.5	4.6	4.2×10^{-5}	0.35
		1	9.2	1.2×10^{-4}	0.48
		2	18	3.7×10^{-4}	0.62
		4	37	1.1×10^{-3}	0.81
		8	74	3.6×10^{-3}	1.0
NIH 3T3	$\beta = 0.24 \pm 0.05$	0.1	0.92	4.3×10^{-6}	3.4×10^{-4}
		0.25	2.3	1.5×10^{-5}	5.7×10^{-4}
		0.5	4.6	4.2×10^{-5}	8.3×10^{-4}
		1	9.2	1.2×10^{-4}	1.1×10^{-3}
		2	18	3.7×10^{-4}	1.5×10^{-3}
		4	37	1.1×10^{-3}	1.9×10^{-3}
		8	74	3.6×10^{-3}	2.5×10^{-3}

[a]The fluid properties are evaluated without particles/cells. Note that, for a shear-thinning fluid, the shear viscosity η changes with the flow rate. The viscosity used in the dimensionless numbers has been evaluated at the average shear rate over the channel cross section, $\dot{\gamma} = Q/H^3$.

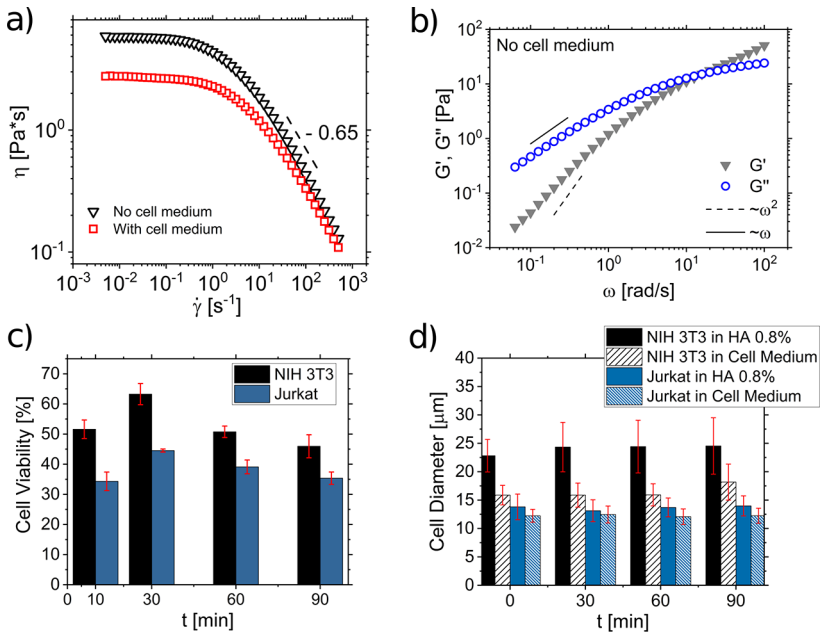

Figure 2. Hyaluronic acid 0.8 wt % solution is strongly shear-thinning and strongly elastic. (a) Shear viscosity η as a function of the shear rate $\dot{\gamma}$ for aqueous HA 0.8 wt % without addition of cell culture medium (black triangles) and with addition of 10 vol % of cell culture medium (red squares). Cell culture medium does not significantly affect the rheology of the fluid (see discussion in Preparation of Cell and Particle Suspensions) Referring to black triangles, a clear shear-thinning region is identified for $\dot{\gamma} > 1\ s^{-1}$, with a flow index of $n = 0.35$ (strongly shear-thinning liquid). (b) Elastic modulus G' and the viscous modulus G'' as a function of the angular frequency ω for the fluid without cell culture medium. Solid and dashed lines are the theoretical slopes for $\omega \to 0$,[25] that is, the terminal region of a viscoelastic liquid. Viability and diameter of cells do not change significantly within 90 min. (c) Cell viability as a function of time for NIH 3T3 (black bars) and Jurkat (blue bars) suspended in HA 0.8 wt %. (d) Cell diameter as a function of time for NIH 3T3 and Jurkat suspended in HA 0.8 wt % (black and blue bars, respectively) and in cell medium (dashed black and dashed blue, for NIH 3T3 and Jurkat cells, respectively). Error bars are evaluated from three independent experiments for each condition.

used to avoid fluid evaporation. The shear viscosity η of HA 0.8 wt % is constant in the range of shear rate $10^{-2} < \dot{\gamma} < 1\ s^{-1}$ (black triangles in Figure 2a). A clear shear-thinning region is identified for $\dot{\gamma} > 1\ s^{-1}$, with a slope of −0.65 corresponding to a

DOI: 10.1021/acs.analchem.7b02450
Anal. Chem. 2017, 89, 13146−13159

flow index n = 0.35, i.e., a strongly shear-thinning liquid. Viscoelastic properties of the HA solution are determined by measuring the elastic modulus G' and the viscous modulus G'' as a function of the angular frequency ω (Figure 2b). HA 0.8 wt % shows strong elastic properties, with $G' < G''$ when $\omega <$ 30 rad/s. Solid and dashed lines are the theoretical slopes of G' and G'' when $\omega \to 0$,[25] that is, the terminal region of a viscoelastic liquid. The intersection of these lines gives an estimate[25] of the longest relaxation time $\lambda \approx 400$ ms. However, since the terminal region is not clearly identified for G', we estimated $\lambda \approx 480$ ms by fitting the viscosity curve of Figure 2a with the Carreau model. The Carreau model[25] describes inelastic fluids with flow-dependent viscosity

$$\eta = \eta_\infty + \frac{\eta_0 - \eta_\infty}{[(1 + (\lambda\dot{\gamma})^2]^{1-n/2}} \quad (5)$$

where η_0 is the zero-shear viscosity, η_∞ is the plateau viscosity at infinite shear (in our case it is zero), λ is the relaxation time, n is the flow index . The value λ = 480 ms is used for the determination of the Deborah number De in the subsequent studies (see Theoretical Background for the definition).

Preparation and Characterization of the Samples. In this work, rigid polystyrene particles with four different diameters and two cell types are used for the transversal migration studies.

Cell Culture. BCL2 (S70A) Jurkat (ATCC CRL-2900) cells are seeded at moderate densities (approximately 7×10^5 cells per flask) in standard 25 cm^2 Corning cell culture flasks (Sigma-Aldrich, Japan). Jurkat cells are cultured in 5 mL of RPMI-1640 (Roswell Park Memorial Institute-1640) culture medium supplemented with 10% fetal bovine serum (both from Thermo Fisher Scientific, Japan) and 200 μg/mL G418 Geneticin (Nacalai Tesque, Inc., Japan) until cells are confluent.

NIH 3T3 (ATCC CRL-1658) fibroblast cells are cultured in a culture medium prepared by reconstituting DMEM (Modified Basal Eagle culture medium) powder (Thermo Fisher Scientific, Japan) in Milli-Q water (Millipore, Japan), which is supplemented with 10% calf serum (Thermo Fisher Scientific, Japan), 3.7 g/L sodium bicarbonate, and 200 μg/mL G418 Geneticin (both from Nacalai Tesque, Inc., Japan). The fibroblast cells are seeded at moderate densities (approximately 7×10^5 cells per flask) in standard 25 cm^2 Corning cell culture flasks and cultured in 5 mL of the prepared and filtered DMEM culture medium until cells become confluent. Both cell types are cultured at 37 °C in 5% CO_2 in a biosafety hood.

Cell Characterizations. Although the absence of PBS in HA 0.8 wt % preserves elastic and shear-thinning properties, it could result in a decrease in cell viability (lack of physiological conditions). Hence, we evaluate the viability of both Jurkat and NIH 3T3 cells in aqueous HA 0.8 wt % and without PBS, over 90 min (Figure 2c). The viability of both cell types suspended in culture medium and PBS are measured to serve as control experiments (Figure S2). Cells suspended in HA 0.8 wt % are first stained with Muse Count & Viability Reagent (1:10 dilution) for 5 min at room temperature, after which the viability is quantified through the flow cytometer Muse Cell Analyzer (Millipore, Japan). Cell viability for both cell types in HA 0.8 wt % does not change significantly within 90 min, being ~38 ± 5% for Jurkat and ~53 ± 7% for NIH 3T3.

As low cell viability could affect cell size,[41] we evaluate the diameter of both cell types over time (Figure 2d). The average cell diameter is determined from phase contrast microscopy images (Figure S3) through an Olympus CKX41 phase-contrast inverted microscope with a 10× objective and equipped with a DP27-A camera system. The combination of lens and camera gives a resolution of ~1.85 pixel/μm. The diameter of both Jurkat and NIH 3T3 suspended in HA 0.8 wt % does not change within 90 min (100 cells analyzed for each condition). Average diameters (over time) are $d = 14 \pm 2$ μm for Jurkat and $d = 24 \pm 5$ μm for NIH 3T3 fibroblasts, suspended in HA 0.8 wt %. Notice also that cells suspended in HA 0.8 wt % are bigger than those suspended in the cell medium, being $d = 12 \pm 1$ μm for Jurkat and $d = 16 \pm 2$ μm for NIH 3T3 (see additional Figure S3 for microscopy images).

Cell stiffness is quantified through the elastic modulus G. Rosenbluth et al.[42] measured the storage modulus of Jurkat cells $G = 0.05 \pm 0.035$ kPa using atomic force microscopy. For NIH 3T3, Bausch et al.[43] determined the storage modulus $20 < G < 40$ kPa using magnetic tweezers. In our analysis, we use G = 20 kPa for NIH 3T3 to evaluate the elastic capillary number Ca_{el} (see Theoretical Background for the definition).

Preparation of Cell and Particle Suspensions. Jurkat cells cultured in the cell culture flasks are counted by standard cell counting procedures using a hemocytometer (Bright-Line, U.S.A.). An appropriate volume of the cell suspension containing 6×10^5 cells is extracted from the flasks and centrifuged at 130g for 5 min to separate the cells from the culture medium. The supernatant is removed, and the cell pellet is resuspended in 50 μL of cell culture medium, added into 500 μL of 0.8 wt % hyaluronic acid solution, and gently mixed to avoid bubbles and cell breakage.

NIH 3T3 cells are adherent cells and grow while being attached to the substrate of the cell culture flasks. As a result, the collection of cells for the preparation of the suspensions requires a further step. Cells are first washed three times with 1 × PBS (phosphate buffer saline) and then incubated with 0.5% trypsin−EDTA mixture (Nacalai Tesque, Inc., Japan) to dissociate the cells from the substrate. An appropriate volume containing 6×10^5 cells is extracted from this mixture after counting by standard cell counting procedures using a hemocytometer. This volume is then centrifuged at 130g for 5 min, after which the supernatant is removed. The cell pellet is resuspended in 50 μL of cell culture medium, added into 500 μL of 0.8 wt % hyaluronic acid, and gently mixed to avoid bubbles and cell breakage.

The addition of 50 μL of cell culture medium introduces both salts and water in 500 μL of 0.8 wt % hyaluronic acid, thus possibly affecting the rheology of the resulting liquid. We then compare the viscosity curve for the liquid with and without cell culture medium (Figure 2a). The slope of the viscosity in the shear-thinning region is preserved and only the shear viscosity η decreases by a factor of 2. Since cell culture medium does not affect significantly the rheology of the fluid, dimensionless numbers presented below are derived by considering the rheology of the fluid without cell culture medium. Note that transversal migration of particles is studied in HA solution without cell culture medium.

Four sets of polystyrene (PS) rigid particles (Polyscience) with diameter d = 6, 10, 15, and 20 μm are added directly to the HA 0.8 wt % at a volume fraction ϕ = 0.01 vol %. The suspension is then put in a vortex mixer to guarantee dispersion and is centrifuged for a couple of seconds to remove air bubbles.

Experiments. A straight square-shaped glass microchannel (Vitrocom, U.S.A.) with channel side H = 100 μm is glued into a silicon tube, directly connected to the needle of the syringe

DOI: 10.1021/acs.analchem.7b02450
Anal. Chem. 2017, 89, 13146−13159

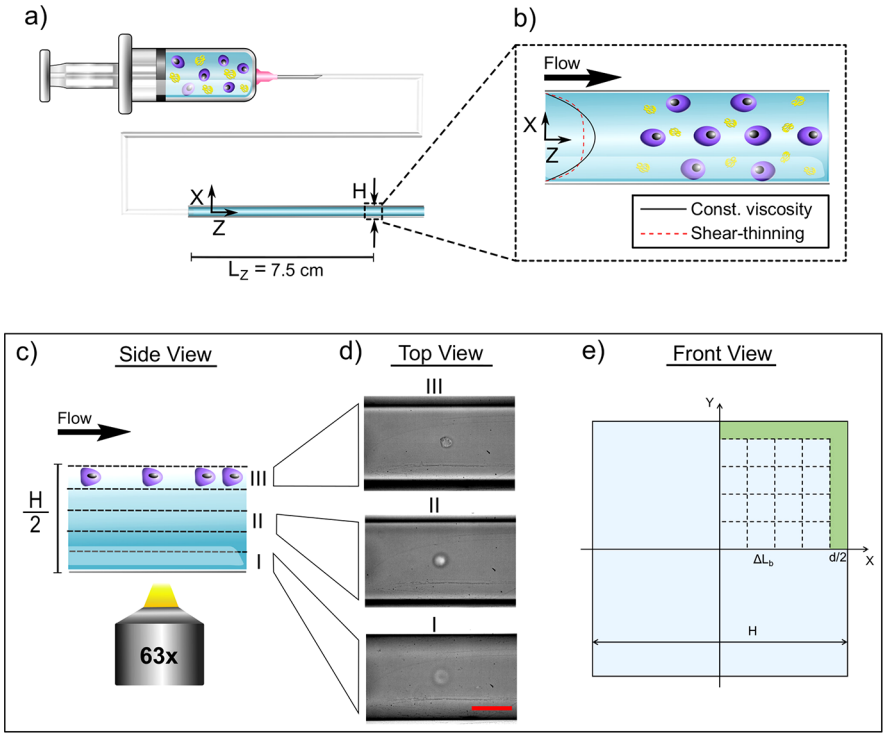

Figure 3. Glass capillary is glued to a silicon tube. (a) Schematic of the experimental apparatus. The square-shaped channel with height $H = 100\ \mu m$ is glued to a silicon tube and then connected directly to the syringe. Velocity profile of shear-thinning fluid is flat around the centerline. (b) Schematic of cells that migrated toward the centerline and the walls as a result of viscoelastic forces. The origin of the Cartesian reference frame is located at the center of the cross section (see also panel (e)). The cross section is identified by the (X, Y) coordinates and Z denotes the main flow direction. In this panel, the velocity field on the X-axis of a constant-viscosity fluid (black line) and of HA 0.8 wt % (red dashed line) are shown. Around the centerline, the velocity profile of the HA 0.8 wt % is flatter than that observed for the constant-viscosity elastic fluid. Velocity profiles are both evaluated at $Q = 0.5\ \mu L/min$ ($De = 4.6$). Cells appear blurred when the lens is outside the focal plane of the cells. (c) Schematic representation explaining the derivation of Y-coordinate of the particles/cells. High magnification lens 63× with a numerical aperture of 0.7 allows distinction between different channel layers along Y (I, II,III). When cells are flowing on the centerline (position III in the side view), if the lens is in focus with the layers I or II, the flowing cells will appear blurred. If the lens is in focus with the layer III, the flowing cells appear optically focused. When the lens is in focus with a given plane, all cells that appear in focus belong to that layer. (d) Top view images are experiments on Jurkat cells at $De = 4.6$, where focal planes are set at 50 μm (I), 20 μm (II), and 0 μm (III) from the center. Position of each layer gives the value of Y. Red scale bar is 50 μm. Square cross section is divided in several bands. (e) Each quadrant of the channel cross section is divided in 4×4 equally sized square subregions k. The green region denotes the zone of the section inaccessible to the particle center. The side length of the bands k depends on the particle diameter and is equal to $\Delta L_b = (H/2 - d/2)/4$.

(Figure 3a). The glass channel has advantages over polydimethylsiloxane (PDMS) devices because of its rigidity. Del Giudice et al.[44] showed that the transversal migration of rigid particles suspended in an aqueous poly(ethylene oxide) solution 1.6 wt % (shear-thinning, $n = 0.5$) differs when the channels are made of PDMS or poly(methyl methacrylate). The authors argued that softer walls (PDMS) alter the dynamics of transversal migration.

The separation experiments of Separation of 10 and 20 μm Particles are carried out in a square-shaped cross section channel made of rigid[44] poly(methyl methacrylate) (PMMA, substrate thickness 1 mm, Kuraray Co. Japan) using a micromilling machine[45] (Minitech CNC Mini-Mill). A 2 mm tip is first used to mill all the substrate to 300 μm to guarantee level uniformity. A 100 μm tip is used to mill the main channel, while the abrupt expansion is milled with a 1 mm tip (see Figure 8a for the schematic of the device). The channel depth is uniform and equal to 100 μm. Finally, two holes are made in the substrate to prepare the access to the inlet and the outlet of the channel. The channel is bonded on another PMMA substrate by immersing the two pieces in absolute ethanol (Sigma-Aldrich) for about 20 min. The two PMMA pieces are then put on a hot press (Imoto IMC-180C, Japan) with plate temperature $T = 40°$ and pressure $P = 0.7$ MPa for about 20 min.

The fluid is pumped through the glass channel at an imposed volumetric flow rate Q using a high precision Harvard PHD-Ultra syringe pump. We used Hamilton gastight glass syringes to avoid wall deformation from affecting the rate of fluid delivery into the microchannel.

The alignment of particles in the microchannel is observed through an inverted microscope (Leica DMIRB) with a 63× Leica air objective and a numerical aperture of 0.7. Images are captured at $L_z = 7.5$ cm from the entrance of the microchannel (the total length of the channel is $L = 10$ cm) using a high speed camera (Phantom Miro M310, Vision Research), at frame rates ranging between 30 and 800 frames per second (fps). Flow stabilization is achieved after ∼15 min. To explore the whole range of the Deborah number $0.92 < De < 74$, experiments with Jurkat and NIH 3T3 cells are carried out in two time intervals, each one no longer than 90 min (cell viability and size do not change within 90 min as discussed in Preparation and Characterization of the Samples). Notice also

DOI: 10.1021/acs.analchem.7b02450
Anal. Chem. 2017, 89, 13146−13159

that cell viability, cell size, and cell migration experiments are carried out within the same day, using the same stock solution.

All the experiments are carried out at room temperature $T = 25 \pm 1$ °C.

Determination of Particle and Cell Distribution along the Channel Cross Section. The strongly shear-thinning nature of HA 0.8 wt % solution makes the evaluation of particle positions difficult. Indeed, previous approaches were based on the evaluation of the off-center distance of the object only[20,22] (i.e., the X-coordinate in Figure 3), or through the comparison between the particle velocities evaluated through particle tracking experiments and numerical simulations[21] to acquire the position of particles or cells on the channel cross section (i.e., both X- and Y-coordinates in Figure 3). Unfortunately, the second approach is not reliable for a strongly shear-thinning fluid such as the one used in the present work. Indeed, this technique evaluates the velocity field $v(X, Y)$ over the channel section through numerical simulations and assumes that the velocity of a particle v_p, evaluated through particle tracking, is equal to the fluid velocity at the particle center. Hence, the X-coordinate is directly measured though microscopy, and the Y-coordinate is obtained by solving the equation $v_p = v(X, Y)$, where v_p is the particle velocity measured through particle tracking experimentally, and $v(X, Y)$ is the velocity profile of the fluid evaluated through numerical simulations.[21,32] However, the equation $v_p = v(X, Y)$ is valid only when the particles are located around the centerline,[46] and the confinement ratio $\beta = d/H \leqslant 0.1$. As shown below, neither of the conditions are satisfied for the system under investigation here. Furthermore, the velocity profile for a strongly shear-thinning fluid is significantly flatter around the channel centerline as compared to that of a fluid with a constant viscosity (compare black solid line with red dashed line in Figure 3b). Thus, the velocities of particles around the channel centerline are very similar, making it hard to distinguish X-positions.

Here, we employ a different methodology to derive the positions of particles and cells during flow. We use a high magnification lens (Leica 63×, aperture of 0.7) with an estimated depth of field of ∼2 μm. When the lens is set on a given focal plane (at a fixed Y in our case), any object in the range of ±1 μm along Y is in focus, while all the other objects located on different focal planes appear to be blurred (middle panel of Figure 3c). We then focus the lens on different focal planes with an increment of 10 μm (layers separated by dashed lines in the left panel of Figure 3c). Any object in focus in a given focal plane belongs to that focal plane, thus univocally identifying Y. For instance, if particles or cells are flowing on the centerline, and the focal plane of the lens is 50 μm (image I in Figure 3d) or 20 μm (image II in Figure 3d) far from the centerline, particles or cells appear to be blurred. If, instead, the focal plane of the lens is set on the centerline (image III in Figure 3d), particles or cells appear optically in focus.

Once the particle positions (X, Y) have been experimentally measured, the particle distribution along the channel cross section can be reconstructed. Following previous works,[21,47] we define the fraction of particles f_k crossing a certain region k of the channel section at a distance L_z from the inlet as

$$f_k(L_z) = \frac{\frac{n_k(L_z)}{A_k \bar{v}_k}}{\sum_k \frac{n_k(L_z)}{A_k \bar{v}_k}} \quad (6)$$

where $n_k(L_z)$ is the number of particles flowing in the band k, and A_k and $\bar{v}_k$ are the cross-sectional area and the average velocity of the band k (fluid without particles), respectively. Here L_z is kept as a constant at $L_z = 7.5$ cm.

We then divide the channel cross section in square subregions (Figure 3e). With reference to the upper-left quadrant, we split the accessible length of both sides of the cross section in four equal segments that form the boundaries of the 4 × 4 bands. The side length of the bands depends on the particle radius and is equal to $\Delta L_b = (H/2 - d/2)/4$. Notice that, with such a subdivision, the areas A_k in eq 6 are equal for any individual band. The average velocities $\bar{v}_k$ have been calculated from the velocity field of the fluid without particles through finite element simulations.[32] Here, the fluid is modeled by the Carreau constitutive equation[48] with parameters obtained by fitting the viscosity curve (Figure 2a). Due to the symmetry of the channel cross section, all the particle/cell positions are moved to the upper-right quadrant ($X > 0$ and $Y > 0$), and the particle fraction distributions are computed only in this quadrant.

EXPERIMENTAL RESULTS

In this section, we report experimental results in terms of fractions of particles over the channel cross section during flow. All the measurements have been taken at a fixed distance from the inlet $L_z = 7.5$ cm. In agreement with previous works,[32] this distance assures that the particles/cells have reached the equilibrium position on the channel section, i.e., no significant change in the particle distribution is found by taking the measurements at a larger distance from the inlet. To further confirm that this distance is sufficiently large, we have estimated the channel length from numerical results available in the literature,[33] assuring that rigid particles attain an equilibrium position. Simulation results refer to a confinement ratio $\beta = 0.1$ and a Deborah number $De = 2.0$. For these parameters, a channel length of about 1.5−2 cm is sufficient to complete the migration process (either to the centerline or to the wall). Higher confinement ratios and Deborah numbers speed up the migration phenomenon so that the required distance from the inlet is even lower.[33] However, we also perform experiments at a lower confinement ratio ($\beta = 0.06$) and Deborah number ($De = 0.92$). By considering the dependence of the migration velocity on De and β reported in the literature (for vanishing De),[17] the length necessary to achieve equilibrium positions at $De = 0.92$ increases 3−4 times. In conclusion, a distance from the inlet $L_z = 7.5$ cm should be sufficient for all the experimental conditions examined in this work.

Typical snapshots for particle and cell suspensions taken with a 10× objective are shown in Figure 4 at two different flow rates (thus Deborah numbers). Following the methodology described in Determination of Particle and Cell Distribution along the Channel Cross Section, the cross-sectional particle/cell positions are reconstructed, and the distributions are then evaluated using a 63× objective. We first describe the results for rigid particles, followed by the analysis for the Jurkat and NIH 3T3 cells.

Rigid Particles. As rigid particles are, by definition, not deformable ($G \to \infty$), the elastic capillary number is $Ca_{el} = 0$. Transversal migration of rigid particles is then driven by purely viscoelastic forces, quantified through the Deborah number De. For $\beta = 0.06$ ($d = 6$ μm) and $De = 0.92$, about 90% of rigid particles are located at the corners of the square cross section, while only ∼5% are found at the band closest to the centerline

DOI: 10.1021/acs.analchem.7b02450
Anal. Chem. 2017, 89, 13146−13159

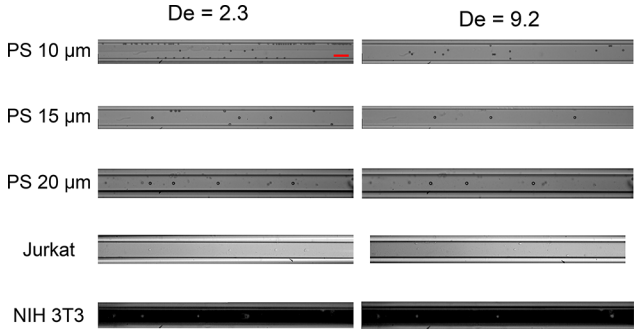

Figure 4. Experimental observation of particle and cell positions. Experimental images of particles and cells at L_z = 7.5 cm from the inlet in the square-shaped microchannel. A 10× objective is used. Images of NIH 3T3 are obtained using phase contrast microscopy. Scale bar is 100 μm. Flow is from left to right.

(Figure 5a1). By fixing β = 0.06 and progressively increasing the Deborah number (that is, by increasing the flow rate Q), the fraction of particles near the corners reduces. For instance, at De = 4.6 (Figure 5a3), the fraction of particles at the corners drops to ∼44%, and the particles migrate near the channel centerline or between the centerline and the walls. From De = 9.2 to De = 74, particles completely migrate away from the corners (Figure 5a4−a7). For β = 0.1 (d = 10 μm), particle distributions are similar to the case of β = 0.06 in the range of 0.92 < De < 4.6 (Figure 5b1−b4). In the range of 4.6 < De < 74, particle distributions at β = 0.1 differ from those found at β = 0.06 (Figure 5b4−b7). Starting from De = 4.6, rigid particles tend to migrate toward the midregion of the channel cross section. At the highest De-value (De = 74) investigated in this work, the equilibrium positions of the particles are evenly distributed along the centerline and close to the midregion of the channel cross section (Figure 5b7).

Rigid particles with a large size β = 0.15 (d = 15 μm) display a different trend. For 0.92 < De < 4.6, particles are driven to both the centerline and the corners of the square cross section (Figure 5c1−c3). As De increases, they progressively align on the centerline until complete 3D focusing is achieved (Figure 5c4−c7). Finally, the largest particles considered in this work (d = 20 μm, β = 0.2) are predominantly aligned on the centerline in the whole range of Deborah number investigated (Figure 5d1−d7). Only at the smallest Deborah number De = 0.92, a small fraction of particles (∼10%) is observed near the corners. We also investigate if particles at β = 0.15 and β = 0.20 remain aligned even at higher flow rates. We find that particles flowing at a flow rate Q = 50 μL/min (De = 460) with β = 0.15 are not tightly focused, while particles with β = 0.2 remain substantially aligned (see Movie S1).

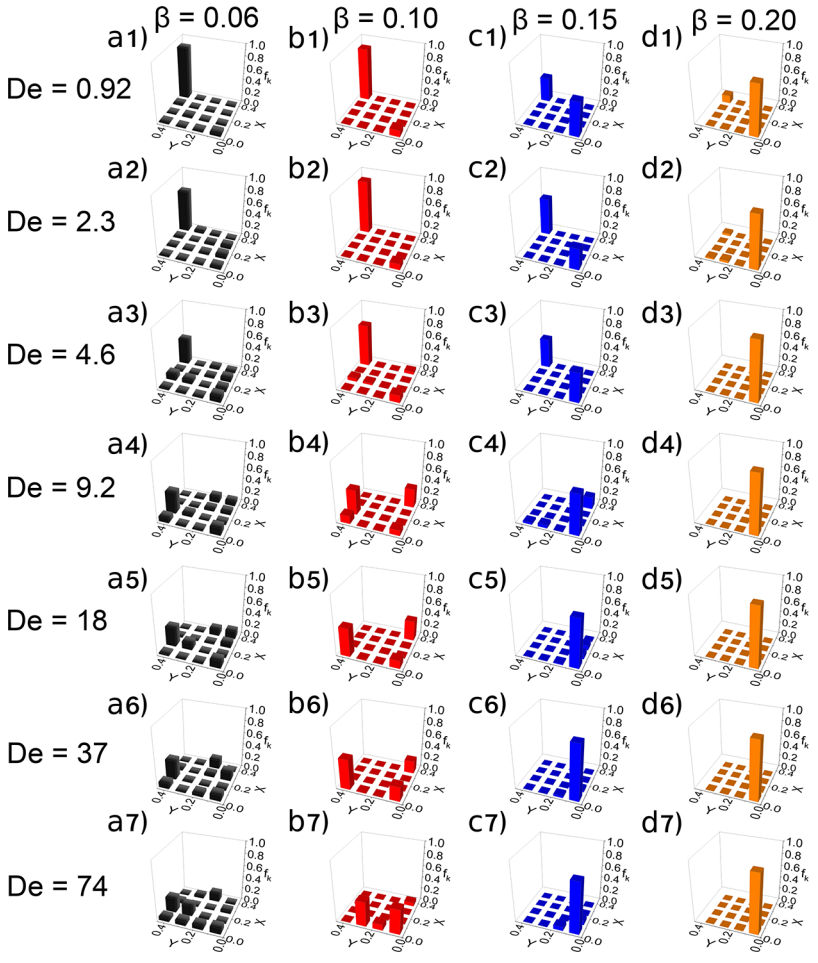

Figure 5. Migration of rigid particles strongly depends on the Deborah number and confinement ratio. Normalized fraction f_k of rigid particles at L_z = 7.5 cm from the inlet as a function of the spatial coordinates XY in the upper-right quadrant of the channel cross section (see Figure 3d). Each row corresponds to a different Deborah numbers De. Each column corresponds to a different confinement ratio β.

DOI: 10.1021/acs.analchem.7b02450
Anal. Chem. 2017, 89, 13146−13159

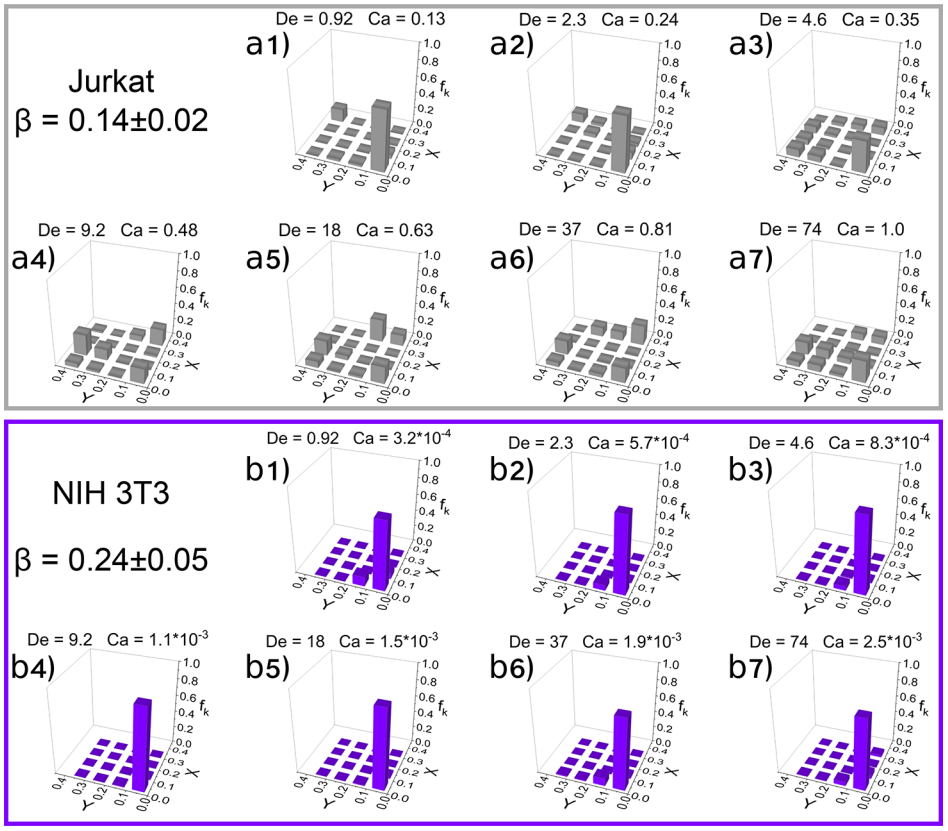

Figure 6. Migration of Jurkat and NIH 3T3 cells depends on confinement ratio and Deborah number. Normalized fraction f_k of cells at L_z = 7.5 cm from the inlet as a function of the spatial coordinates XY in the upper-right quadrant of the channel cross section (see Figure 3d) for different Deborah numbers De. Panels (a1−a7) report the results for Jurkat cells (d = 14 ± 2 μm). Panels (b1−b7) refer to NIH 3T3 cells (d = 24 ± 5 μm).

Cells. Comparing to rigid particles, cells are deformable. As discussed in Theoretical Background, the effect of the deformability-induced force is quantified through the elastic capillary number Ca_{el}. The storage modulus of Jurkat cells is estimated to be G = 0.05 ± 0.035 kPa,[42] while the storage modulus of NIH 3T3 is estimated to be $G \approx 20$ kPa.[43] These values of G correspond to the range of elastic capillary number $0.13 < Ca_{el} < 1$ for Jurkat cells and $3.4 \times 10^{-4} < Ca_{el} < 2.5 \times 10^{-3}$ for NIH 3T3. Hence, the effect of shape deformation on the lateral motion of cells is expected to be stronger for Jurkat than for NIH 3T3 cells.

The average diameter of Jurkat cells in HA 0.8 wt % is d = 14 ± 2 μm, thus β = 0.14 ± 0.02. Jurkat cells are prevalently focused on the channel centerline in the range of Deborah numbers $0.92 < De < 2.6$ (Figure 6a1,a2). At Deborah numbers in the range $4.6 < De < 74$, cells are found to enrich positions in the vicinity of the walls (Figure 6a3−a7). Positions of Jurkat cells along the square cross section are similar to those of rigid particles with β = 0.15 in the range $0.91 < De < 2.3$, while they bare more similarity to those observed for rigid particles at β = 0.1 when $9.2 < De < 74$. This is not surprising since the diameter of Jurkat cells spans the range $12 < d < 16$ μm. The deformability-induced force is also expected to play a role in the migration process. Indeed, we observe highly deformed cells near the walls and less deformed cells on the centerline (Figure S4 for cells flowing at De = 74). Such difference in the observed deformability is related to the velocity profile for shear-thinning liquids (flat around the centerline).

The average diameter of NIH 3T3 cells is d = 24 ± 5 μm, thus β = 0.24 ± 0.05. NIH 3T3 cells align on the channel centerline in the whole range of the Deborah number investigated, $0.91 < De < 74$ (Figure 6b1−b7). Comparing these results with those for rigid particles at β = 0.2, we found a strong similarity between the equilibrium positions over the channel cross section attained by rigid particles and NIH 3T3 cells.

DISCUSSION

Transversal Migration of Rigid Particles. The transversal migration of rigid particles in a strongly shear-thinning liquid can be summarized as follows: (i) at a fixed Deborah number De, the fraction of particles aligned on the channel centerline increases with increasing particle size (i.e., confinement ratio β), whereas the fraction of particles at the corners decreases. Equilibrium positions are then shifted from the corners to the centerline, i.e.,"from the edge to the center"; (ii) at a fixed β, the fraction of particles at the corners decreases with increasing Deborah number De; (iii) for relatively low values of $0.06 < \beta < 0.1$, rigid particles attain an equilibrium position between the wall and the centerline; (iv) larger particles (i.e., large β) prevalently migrate toward the channel centerline, and this effect is enhanced at high Deborah numbers.

It is worthwhile to mention that, even at the lowest De-value, the maximum estimated shear rate in the channel (at the wall) falls in the shear-thinning region. As De increases, the maximum shear rate increases as well, and a larger volume of fluid is characterized by a viscosity lower than its zero-shear value.

Our observations at low confinement ratios and Deborah numbers (i.e., migration toward the corners) are consistent with previous experimental and numerical studies dealing with

DOI: 10.1021/acs.analchem.7b02450
Anal. Chem. 2017, 89, 13146−13159

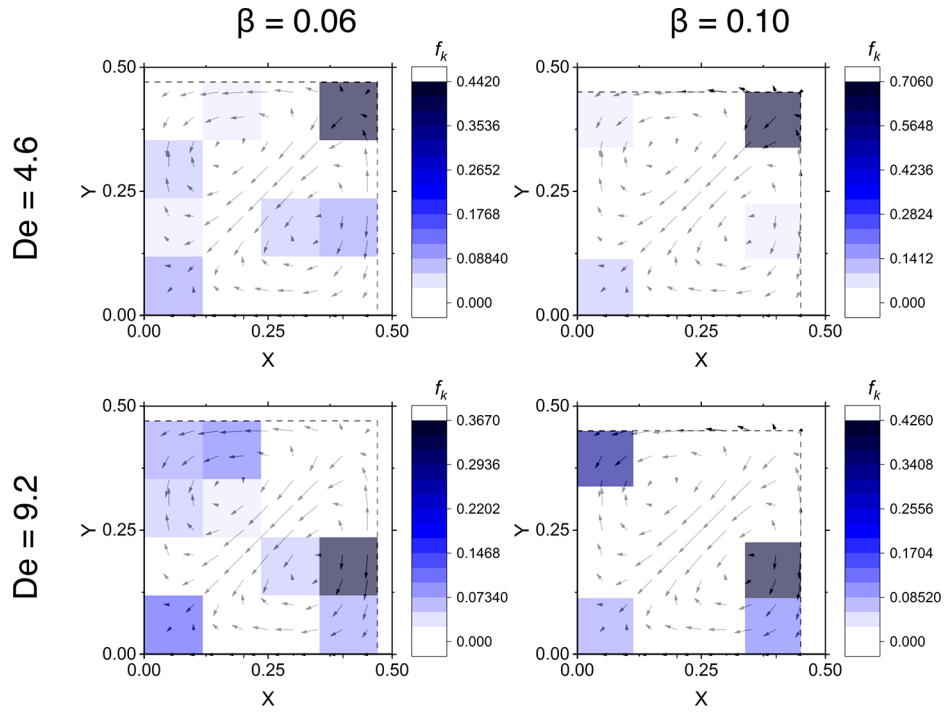

Figure 7. Positions of particles match with the predicted positions of viscoelastic vortices. Velocity field over the channel cross section of 0.8 wt % hyaluronic acid solution derived from numerical simulations (details can be found in SI). The color bars on the lateral side indicate the normalized fraction of particles as in eq 6. Solid dashed lines delimitate the zone accessible by the particle. Good agreement is found between the position of particles and the predicted position of the vortices induced by the viscoelastic secondary flows.

weaker shear-thinning fluids. Song et al.[22] studied the transversal migration of rigid particles with $\beta \approx 0.1$. They found that particles suspended in weakly shear-thinning poly(ethylene oxide) solutions migrated toward the channel centerline when exploring the constant-viscosity zone of the viscoelastic suspending fluid, whereas particles deviated from the channel axis as the flow rate becomes sufficiently high to enhance the shear-thinning of the suspending culture medium. Very recently, Li et al.[37] found results similar to Song et al.[22] for the migration of rigid particles in a weakly shear-thinning hyaluronic acid solution flowing in a straight microchannel with aspect ratio (width over height) varying between 1 and 3. Li et al.[37] also observed a strong dependence of the elastic migration force on the polymer concentration and confinement ratio. Seo et al.[31] studied migration of particles suspended in 1 wt % PEO solution ($n = 0.65$) under two conditions: (i) when inertial and viscoelastic forces were comparable and (ii) when inertial forces dominated. When inertial and elastic forces were comparable, they found that particles were focused to the centerline and near the walls at $\beta = 0.1$ but only to the centerline at $\beta = 0.17$. When inertial forces dominate, particles were dispersed around the centerline for $\beta = 0.1$, but were focused at the centerline for $\beta = 0.17$. However, they did not observe a complete shifting in the particle positions when increasing the particle size. Different from their work, inertial effects are negligible in our experiments (Table 1). Villone et al.[33] numerically studied the transversal migration of a single particle suspended in a strongly shear-thinning viscoelastic liquid described by the Phan-Thien Tanner model. (The Phan-Thien Tanner model[49] describes polymer solutions presenting shear-thinning and first normal stress difference, while it predicts a null second normal stress difference.) They found that the particles migrate toward the centerline or the corners of a straight channel depending on *De*. At $De < 1$, i.e., when exploring the constant-viscosity zone of the fluid, particles migrate mainly toward the channel centerline regardless of the initial position. Only particles that start very close to the walls migrate toward the corners. At $De > 1$, i.e., in the shear-thinning zone, particles migrate toward both the channel centerline and the walls, or toward the corners only. Finally, Del Giudice et al.[32] found that particles suspended in a poly(ethylene oxide) 1.6 wt % solution (shear-thinning fluid, flow index $n = 0.5$) with $\beta = 0.1$ were well focused at the corners of the square-shaped microchannel at $De = 9.2$. In this work, we find that migration toward the corners occurs at a much lower Deborah number ($De = 0.92$). However, the fluid used in the present work has a lower flow index ($n = 0.35$), thus suggesting that the strength of shear-thinning affects the transversal migration toward the corners.

As the Deborah number increases, the particles migrate away from the corners (Figure 5a3−a7) and Figure 5b3−b7). In contrast, previous experimental[32,37] and numerical[33] results have shown that the transversal migration toward the corners is enhanced by increasing *De*. The detachment of particles from the walls has previously been associated with the inertial wall-lift force that is relevant at high flow rates. The importance of inertial forces is quantified through the Reynolds number *Re*. Di Carlo[11] reported that inertial effects become dominant as $Re \approx 1$. As reported in Table 1, the highest Reynolds number in our experiments is $Re = 3.6 \times 10^{-3}$, thus inertial effects are irrelevant in our case. A possible explanation that might justify our experimental observations is the possible occurrence of secondary flows on the channel cross section. These flows lead to the formation of vortices near the four corners of the square channel section and are caused by a viscoelastic property called second normal stress difference. An extensive investigation on the effect of secondary flows on the particle lateral motion has

DOI: 10.1021/acs.analchem.7b02450
Anal. Chem. 2017, 89, 13146−13159

been carried out by Villone et al.[33] through numerical simulations, using the Giesekus model to describe the viscoelastic fluid. (The Giesekus model[50] describes polymer solutions presenting shear-thinning, positive first normal stress difference, and negative second normal stress difference.) They found that, if the confinement ratio was sufficiently low ($\beta \leq 0.1$), these vortices "attract" a small fraction of the particles, leading to an additional equilibrium particle position between the channel centerline and the walls. For $\beta = 0.1$ and $De = 6$ (higher values of De are not reported in their work), Villone et al.[33] predicted this extra equilibrium position in the region around $(X, Y) = (0.18, 0.35)$, in very good quantitative agreement with the position $(X, Y) = (0.17, 0.4)$ observed from our measurements, corresponding to a peak in the particle fraction. We also carried out numerical simulations to evaluate the position of viscoelastic vortices along the cross section for our 0.8 wt % HA solution (Figure 7). Hyaluronic acid solution has been modeled through the Giesekus model (details can be found in the Supporting Information (SI)). We compared the position of viscoelastic vortices with particle positions at $\beta = 0.06$ and $\beta = 0.1$ for $De = 4.6$ and $De = 9.2$ (colored squares in Figure 7). We find that the position of viscoelastic vortices is in good agreement with the experimentally observed peaks in the particle fraction.

As the confinement ratio increases, particles are driven toward the corners and the centerline up to $De = 4.6$ and progressively align around the centerline at higher De-values. Villone et al.[33] reported that, by increasing the confinement ratio β, a significant variation in the equilibrium positions attained by the particles emerges. Specifically, larger particles are not influenced by the secondary flows anymore (the extra equilibrium position generated by the presence of the vortices disappears) and tend to migrate toward the centerline. Remarkably, at higher confinement ratio $\beta \geqslant 0.15$, no particles are observed between the channel centerline and the walls, in agreement with the numerical findings.

A direct measurement of a nonzero second normal stress difference for the HA 0.8 wt % solution would strengthen our argument above. Unfortunately, such a measure cannot be easily performed due to (i) lack of a well-established method to make this measurement feasible; (ii) low normal stress values of this fluid (the second normal stress difference is generally 1 order of magnitude lower than the first normal stress difference, which is already low for the 0.8 wt % HA solution). Nevertheless, the agreement with numerical simulations supports our argument that the existence of secondary flows is a plausible explanation for our experimental observations.

Transversal Migration of Cells. The heterogeneous nature of cells[51] does not allow us to definitely settle the origin behind the positions observed in our experiments. However, we wish to compare our experimental results with simulation on deformable objects in shear-thinning liquids presented by Villone et al.[36]

The migration of Jurkat cells is significantly affected by the heterogeneity of cell diameters (rigid particles show very different migration trends at $\beta = 0.1$ and $\beta = 0.15$, which are the same values of the confinement ratios for Jurkat cells). In the range of Deborah number $0.92 < De < 2.3$, Jurkat cells are mainly aligned on the channel centerline (Figure 6a1,a2). In particular, the fraction of Jurkat cells on the corners at $De = 0.92$ is $f_k = 0.16$, which is lower than both the fraction of rigid particles in the corners at $\beta = 0.1$ ($f_k = 0.88$) and at $\beta = 0.15$ ($f_k = 0.49$). This migration trend can be ascribed to both the effect of the confinement (for bigger cells) and to the deformability-induced force acting on Jurkat cells. Yang et al.[23] experimentally observed that red blood cells (average elastic modulus $G = 0.75 \pm 12$ kPa[52] is much higher than $G = 0.05 \pm 0.035$ kPa for Jurkat cells) suspended in a near constant-viscosity liquid experienced such deformability-induced force, promoting transversal migration toward the centerline. In shear-thinning liquids, numerical simulations[33] and experiments[37] showed that the elastic force promotes migration toward the centerline or the corners of the square-shaped microchannel depending on the initial position of the cells (see also Theoretical Background). Therefore, competition or synergy between elastic and deformability-induced force is expected. Villone et al.[36] carried out numerical simulations of elastic particles with $\beta = 0.2$ in shear-thinning liquids (modeled through the Giesekus model[50]). They found that an elastic particle with $\beta = 0.2$ migrated toward the channel centerline when the elastic capillary number $Ca_{el} > 0.1$ in the range of the Deborah number $0.2 < De < 1$, in very good agreement with our findings for the transversal migration of Jurkat cells when $0.13 < Ca_{el} < 0.24$. At higher De and Ca_{el}, bigger Jurkat cells are supposed to remain aligned on the centerline due to the high confinement (as for rigid particles at $\beta = 0.15$), while smaller Jurkat cells are supposed to remain on the centerline because of the deformability-induced force. On the contrary, we observe Jurkat cells on the centerline and on positions close to the channel wall. These findings can be justified as follows. When increasing the Deborah number De by increasing the flow rate, the elastic capillary number Ca_{el} increases as well. However, increasing the Deborah number De by a factor of 2 corresponds to a mere increase of maximum 33% in Ca_{el} (see Table 1) because the viscosity decreases. In other words, as the flow rate increases, the increase in fluid elastic force is far more significant than the increase in deformability-induced force. As reported in Theoretical Background, when increasing De, the neutral plane approaches more toward the centerline, thus most of the cells would likely migrate away from the centerline. However, the deformability-induced force also increases and is directed toward the centerline. As a consequence, a competition between elastic forces and deformability-induced forces is expected to modify equilibrium positions. Our experiments show that cells occupy positions qualitatively similar to rigid particles at $\beta = 0.1$ in the range of Deborah number $9.2 < De < 74$, thus suggesting that the viscoelastic force overcomes the deformability-induced force, allowing migration toward the wall. Numerical simulations of Villone et al.[36] did not explore such high values of Deborah number nor other confinement ratios, thus further comparison is not currently possible.

NIH 3T3 are much stiffer than Jurkat cells, since the elastic modulus of NIH 3T3 is $G \approx 20$ kPa.[52] The highest elastic capillary number found in our experiments for NIH 3T3 is $Ca_{el} = 2.5 \times 10^{-3}$, and numerical simulations of Villone et al.[36] reported that deformability-induced force is negligible at such value of Ca_{el}. In our experiments, NIH 3T3 cells follow the same migration trend of rigid particles with $\beta = 0.2$, in agreement with numerical simulations of Villone et al.[33] for the transversal migration of elastic particles at vanishing capillary numbers, suggesting that the deformability-induced force is negligible.

Recalling that average cell viability in our experiments is ~50%, a fraction of dead cells is also tracked during our measurements, contributing to the distribution of their positions (Figure 6). It is worth discussing whether dead cells

DOI: 10.1021/acs.analchem.7b02450
Anal. Chem. 2017, 89, 13146−13159

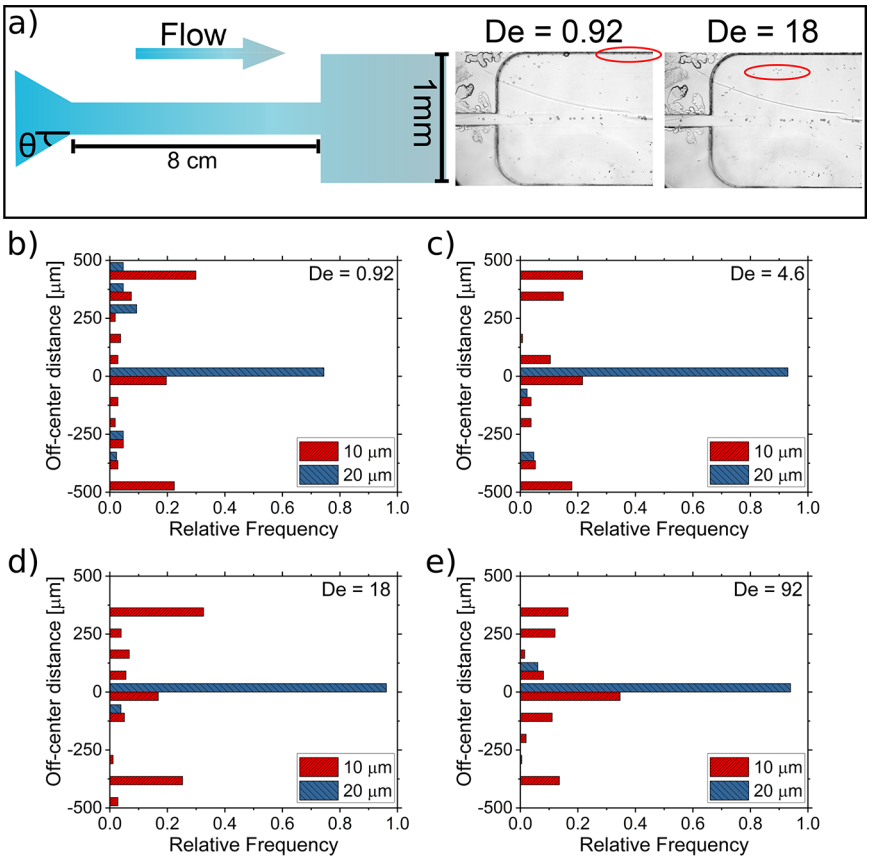

Figure 8. Particles with diameters of 10 and 20 μm are separated in a straight channel with an abrupt expansion. (a) Schematic of the PMMA microfluidic device (see fabrication details in Experiments) with relevant dimensions (θ = 20°, dimensions not in scale). Experimental images at De = 0.92 and De = 4.6 are also reported. Red circles highlight 10 μm particles. (b–e) Frequency distribution of particles along X coordinate (i.e., upper view) at several Deborah numbers (see also Movie S2).

experience a different deformability-induced force as compared to living cells, as the value of the elastic modulus G used in this work refers to living cells. Unfortunately, we have no indication about the G-value pertaining to dead cells. If dead cells were assumed to be softer than living cells, they would experience a stronger deformability-induced force, thus making our estimate of the capillary number Ca_{el} conservative. On the contrary, if dead cells were assumed to be stiffer than living cells, our value of Ca_{el} is overestimated. However, we find a different behavior between the transversal migration of deformable Jurkat cells and that of rigid particles ($G \rightarrow \infty$). Thus, the migration dynamics of dead cells, even if stiffer, must still be significantly affected by deformability.

Separation of 10 and 20 μm Particles. Position of particles can be shifted "from the edge to the center" by properly tuning the confinement ratio β in a strongly shear-thinning liquid (Figure 5). In particular, 10 μm particles tend to migrate in the vicinity of the wall, while 20 μm particles tend to migrate toward the channel centerline. Therefore, separation between these two sets of particles can be achieved in a straight microfluidic channel. In order to enhance the distance between the streamlines on which particles of different sizes are located, an abrupt expansion can be subsequently added. We have designed a PMMA (rigid material) microfluidic device made of a straight channel connected to an abrupt expansion (Figure 8a). At De = 0.92, 10 μm particles are prevalently focused at the corners of the abrupt expansion (red circles in Figure 8a), while 20 μm particles are focused at the centerline, in agreement with our observation in straight glass channels with square cross sections (Figure 5). At De = 18, 10 μm particles detach from the corner but are still focused in the vicinity of the walls of the abrupt expansion, while 20 μm particles are focused at the centerline, again in good agreement with our observations in glass capillary (Figure 5). We demonstrate that 10 μm particles can be separated from 20 μm particles in a simple straight channel with an abrupt expansion (Figure 8b–e and Movie S2). Notice that particles are better separated in the range of Deborah number of 0.92 < De < 18 (Figure 8b–d). A further increase of the Deborah number to De = 92, leads to an increase of 10 μm particles in the central plane (Figure 8e) of the microfluidic device, consistent with our previous observations in a glass channel (Figure 5). At De = 18 (best separation efficiency observed), the separation efficiency is ~96% for 20 μm particles and ~80% for 10 μm particles (Figure 8c).

CONCLUSIONS

In this work, we studied the transversal migration of particles and cells suspended in a viscoelastic, strongly shear-thinning liquid flowing in a straight square-shaped microchannel. We used rigid particles with four different sizes and two types of cells, namely Jurkat cells and NIH 3T3 fibroblasts. The suspending liquid is an aqueous solution of 0.8 wt % hyaluronic acid, with a flow index n = 0.35.

We show that the equilibrium positions over the channel cross section attained by the particles can be shifted "from the edge to the center" without changing the suspending liquid.

DOI: 10.1021/acs.analchem.7b02450
Anal. Chem. 2017, 89, 13146–13159

Specifically, regarding the rigid particle suspensions at relatively low confinement ratios ($\beta = 0.06$ and $\beta = 0.1$), lateral migration is toward the corners or the middle plane of the microchannel as a function of the Deborah number De (related to the flow rate Q). We also infer that secondary viscoelastic vortices in the proximity of the corners can affect particle migration, in agreement with previous numerical simulations.[33] Larger particles ($\beta = 0.15$ and $\beta = 0.2$) preferentially migrate toward the centerline. Particles at $\beta = 0.2$ remain aligned to the centerline even at flow rates $Q = 50$ μL/min ($De = 460$). Jurkat cells ($\beta = 0.14 \pm 0.02$) migrate toward the channel centerline or the walls, as a function of both the Deborah number De and the elastic capillary number Ca_{el}. NIH 3T3 cells ($\beta = 0.24 \pm 0.05$) migrate toward the channel centerline in the whole range of Deborah numbers investigated. We argue that transversal migration of Jurkat (soft) cells is also affected by deformability-induced force. Finally, separation of 10 and 20 μm particles is achieved in a straight microchannel with an abrupt expansion.

To conclude, we would like to suggest future directions and envisage the impact of our findings on viscoelasticity-based microfluidics. A model able to describe the elastic force in shear-thinning liquids as a function of the dimensionless numbers presented here is not yet available. Our experimental methodology would allow an in-depth investigation of several fluid-particle combinations. The competition between deformability-induced force and viscoelastic force on the transversal migration of cells in strongly shear-thinning liquids could be further clarified by studying other cell types with different sizes and deformability, such as mammalian cells or red blood cells. To this aim, some effort should be made to increase cell viability in strongly shear-thinning liquids. Addition of phosphate buffer saline is expected to increase cell viability but is also expected to decrease the shear-thinning strength.[40] Theoretical works[38] suggest that an increase in polymer concentration will balance the detrimental effect of PBS on fluid elasticity. In this regard, our viability experiments on Jurkat and NIH 3T3 cells suspended in hyaluronic acid in PBS (Figure S2) suggests that HA does not affect cell viability.

The results on the migration trends at $\beta = 0.15$ for rigid particles and Jurkat cells ($\beta = 0.14 \pm 0.02$) when $De > 9.2$ support our argument that separation of cells with different deformability but comparable size, useful in biomedical applications such as separation of blood components or separation of healthy from cancer cells,[1−3] can be achieved.

Very recently, dynamics of particles and droplets at the interface between immiscible liquids have been studied.[53,54] Two novel methodologies for particle separation[55] and washing[56] using a coflow of weakly viscoelastic fluids and Newtonian fluids has also been presented. Further studies with shear-thinning liquids would allow the design of novel coflow microfluidic devices for particles and droplet separation.

Finally, we believe that our findings will motivate further investigation on viscoelastic ordering of particles and cells in microfluidic devices. In this regard, D'Avino et al.[57] showed through numerical simulations that, at high Deborah numbers, two or three particles aligned along the channel centerline tend to separate until they reach an equilibrium distance. Although the numerical analysis has been limited to a very few number of objects, the results seem to encourage the possibility to generate equally spaced particle trains. Viscoelastic ordering of particles and cells will lead to a large number of novel applications, such as highly efficient particle and cell encapsulation for microfluidic drop sequencing.[58]

■ ASSOCIATED CONTENT

Supporting Information

The Supporting Information is available free of charge on the ACS Publications website at DOI: 10.1021/acs.analchem.7b02450.

Alignment of 15 and 20 μm particles at several volumetric flow rates (Movie S1); separation of 10 and 20 μm particles at $Q = 0.1$ μL/min and $Q = 2$ μL/min (Movie S2) (ZIP)

Comparison between the flow curves of 0.8 wt % HA in water and in PBS (Figure S1); viability of Jurkat cells as a function of time in several suspending fluids (Figure S2); phase contrast microscopy images of Jurkat cells and of NIH 3T3 fibroblasts (Figure S3); experimental images of deformed cells (Figure S4); description of the mathematical model and numerical simulations (Supporting Information S1); values of the constitutive parameters used in the simulations (Table S1) (PDF)

■ AUTHOR INFORMATION

Corresponding Authors

*E-mail: francesco.delgiudice@me.com (F.D.G.)

*E-mail: amy.shen@oist.jp (A.Q.S.)

ORCID

Francesco Del Giudice: 0000-0002-9414-6937

Amy Q. Shen: 0000-0002-1222-6264

Notes

The authors declare no competing financial interest.

■ ACKNOWLEDGMENTS

The authors thank Professor Pier Luca Maffettone, Professor Abraham Lee, and Professor Dino Di Carlo for useful discussions. Mr. Kei Funakoshi from the Micro/Bio/Nanofluidics Unit at OIST is acknowledged for his help with the fabrication of the PMMA device. F.D.G., S.S., and A.Q.S. gratefully acknowledge the support of the Okinawa Institute of Science and Technology Graduate University with subsidy funding from the Cabinet Office, Government of Japan. A.Q.S. also acknowledge funding from the Japan Society for the Promotion of Science, Grants-in-Aid for Scientific Research (C), grant number 17K06173.

■ REFERENCES

(1) Bhagat, A. A. S.; Bow, H.; Hou, H. W.; Tan, S. J.; Han, J.; Lim, C. T. *Med. Biol. Eng. Comput.* **2010**, *48*, 999−1014.

(2) Gossett, D. R.; Weaver, W. M.; Mach, A. J.; Hur, S. C.; Tse, H. T. K.; Lee, W.; Amini, H.; Di Carlo, D. *Anal. Bioanal. Chem.* **2010**, *397*, 3249−3267.

(3) Hur, S. C.; Henderson-MacLennan, N. K.; McCabe, E. R.; Di Carlo, D. *Lab Chip* **2011**, *11*, 912−920.

(4) Xuan, X.; Zhu, J.; Church, C. *Microfluid. Nanofluid.* **2010**, *9*, 1−16.

(5) Dannhauser, D.; Rossi, D.; Causa, F.; Memmolo, P.; Finizio, A.; Wriedt, T.; Hellmers, J.; Eremin, Y.; Ferraro, P.; Netti, P. *Lab Chip* **2015**, *15*, 3278−3285.

(6) Wang, G.; Mao, W.; Byler, R.; Patel, K.; Henegar, C.; Alexeev, A.; Sulchek, T. *PLoS One* **2013**, *8*, e75901.

(7) Pethig, R. *Biomicrofluidics* **2010**, *4*, 022811.

(8) Pamme, N. *Lab Chip* **2006**, *6*, 24−38.

(9) Friend, J.; Yeo, L. Y. *Rev. Mod. Phys.* **2011**, *83*, 647.

(10) Di Carlo, D.; Irimia, D.; Tompkins, R. G.; Toner, M. *Proc. Natl. Acad. Sci. U. S. A.* **2007**, *104*, 18892−18897.

(11) Di Carlo, D. *Lab Chip* **2009**, *9*, 3038−3046.

DOI: 10.1021/acs.analchem.7b02450
Anal. Chem. 2017, 89, 13146−13159

(12) Di Carlo, D.; Edd, J. F.; Humphry, K. J.; Stone, H. A.; Toner, M. *Phys. Rev. Lett.* [Online] **2009**, *102*.10.1103/PhysRevLett.102.094503
(13) Choi, Y.-S.; Seo, K.-W.; Lee, S.-J. *Lab Chip* **2011**, *11*, 460−465.
(14) Hur, S. C.; Tse, H. T. K.; Di Carlo, D. *Lab Chip* **2010**, *10*, 274−280.
(15) Kunze, A.; Che, J.; Karimi, A.; Di Carlo, D. *Lab Chip* **2015**, *15*, 605−609.
(16) Lu, X.; Liu, C.; Hu, G.; Xuan, X. *J. Colloid Interface Sci.* **2017**, *500*, 182.
(17) D'Avino, G.; Greco, F.; Maffettone, P. L. *Annu. Rev. Fluid Mech.* **2017**, *49*, 341−360.
(18) Faridi, M. A.; Ramachandraiah, H.; Banerjee, I.; Ardabili, S.; Zelenin, S.; Russom, A. *J. Nanobiotechnol.* [Online] **2017**, *15*.10.1186/s12951-016-0235-4
(19) Leshansky, A.; Bransky, A.; Korin, N.; Dinnar, U.; *Phys. Rev. Lett.* [Online] **2007**, *98*.10.1103/PhysRevLett.98.234501
(20) Yang, S.; Kim, J. Y.; Lee, S. J.; Lee, S. S.; Kim, J. M. *Lab Chip* **2011**, *11*, 266−273.
(21) Del Giudice, F.; Romeo, G.; D'Avino, G.; Greco, F.; Netti, P. A.; Maffettone, P. L. *Lab Chip* **2013**, *13*, 4263−4271.
(22) Song, H. Y.; Lee, S. H.; Salehiyan, R.; Hyun, K. *Rheol. Acta* **2016**, *55*, 889−900.
(23) Yang, S.; Lee, S. S.; Ahn, S. W.; Kang, K.; Shim, W.; Lee, G.; Hyun, K.; Kim, J. M. *Soft Matter* **2012**, *8*, 5011−5019.
(24) Kim, B.; Kim, J. M. *Biomicrofluidics* **2016**, *10*, 024111.
(25) Macosko, C. W.; Larson, R. G. Nonlinear Viscoelasticity. *Rheology: Principles, Measurements, And Applications*; Wiley-VCH: New York, 1994; pp 135−174.
(26) Lindner, A.; Bonn, D.; Meunier, J. *Phys. Fluids* **2000**, *12*, 256−261.
(27) Lim, E. J.; Ober, T. J.; Edd, J. F.; Desai, S. P.; Neal, D.; Bong, K. W.; Doyle, P. S.; McKinley, G. H.; Toner, M. *Nat. Commun.* **2014**, *5*.10.1038/ncomms5120
(28) Nam, J.; Tan, J. K. S.; Khoo, B. L.; Namgung, B.; Leo, H. L.; Lim, C. T.; Kim, S. *Biomicrofluidics* **2015**, *9*, 064117.
(29) Liu, C.; Xue, C.; Chen, X.; Shan, L.; Tian, Y.; Hu, G. *Anal. Chem.* **2015**, *87*, 6041−6048.
(30) Yuan, D.; Tan, S. H.; Zhao, Q.; Yan, S.; Sluyter, R.; Nguyen, N.-T.; Zhang, J.; Li, W. *RSC Adv.* **2017**, *7*, 3461−3469.
(31) Seo, K. W.; Kang, Y. J.; Lee, S. J. *Phys. Fluids* **2014**, *26*, 063301.
(32) Del Giudice, F.; D'Avino, G.; Greco, F.; Netti, P. A.; Maffettone, P. L. *Microfluid. Nanofluid.* **2015**, *19*, 95−104.
(33) Villone, M.; D'Avino, G.; Hulsen, M.; Greco, F.; Maffettone, P. *J. Non-Newtonian Fluid Mech.* **2013**, *195*, 1−8.
(34) Li, G.; McKinley, G. H.; Ardekani, A. M. *J. Fluid Mech.* **2015**, *785*, 486−505.
(35) Wang, C. J.; Li, X.; Lin, B.; Shim, S.; Ming, G.-l.; Levchenko, A. *Lab Chip* **2008**, *8*, 227−237.
(36) Villone, M. M.; Greco, F.; Hulsen, M. A.; Maffettone, P. L. *J. Non-Newtonian Fluid Mech.* **2016**, *234*, 105−113.
(37) Li, D.; Lu, X.; Xuan, X. *Anal. Chem.* **2016**, *88*, 12303−12309.
(38) Dobrynin, A. V.; Colby, R. H.; Rubinstein, M. *Macromolecules* **1995**, *28*, 1859−1871.
(39) Rubinstein, M.; Colby, R. H. *Polymer Physics*; Oxford University Press: Oxford, U.K., 2003.
(40) Del Giudice, F.; Calcagno, V.; Esposito Taliento, V.; Greco, F.; Netti, P. A.; Maffettone, P. L. *J. Rheol.* **2017**, *61*, 13−21.
(41) Ziegler, U.; Groscurth, P. *News Physiol. Sci.* **2004**, *19*, 124−128.
(42) Rosenbluth, M. J.; Lam, W. A.; Fletcher, D. A. *Biophys. J.* **2006**, *90*, 2994−3003.
(43) Bausch, A. R.; Ziemann, F.; Boulbitch, A. A.; Jacobson, K.; Sackmann, E. *Biophys. J.* **1998**, *75*, 2038−2049.
(44) Del Giudice, F.; Greco, F.; Netti, P. A.; Maffettone, P. L. *Biomicrofluidics* **2016**, *10*, 043501.
(45) Guckenberger, D. J.; de Groot, T. E.; Wan, A. M.; Beebe, D. J.; Young, E. W. *Lab Chip* **2015**, *15*, 2364−2378.
(46) Higdon, J.; Muldowney, G. *J. Fluid Mech.* **1995**, *298*, 193−210.
(47) Romeo, G.; D'Avino, G.; Greco, F.; Netti, P. A.; Maffettone, P. L. *Lab Chip* **2013**, *13*, 2802−2807.
(48) Bird, R. B.; Carreau, P. J. *Chem. Eng. Sci.* **1968**, *23*, 427−434.
(49) Thien, N. P.; Tanner, R. I. *J. Non-Newtonian Fluid Mech.* **1977**, *2*, 353−365.
(50) Giesekus, H. *J. Non-Newtonian Fluid Mech.* **1982**, *11*, 69−109.
(51) Yin, H.; Marshall, D. *Curr. Opin. Biotechnol.* **2012**, *23*, 110−119.
(52) Girard, P. P.; Cavalcanti-Adam, E. A.; Kemkemer, R.; Spatz, J. P. *Soft Matter* **2007**, *3*, 307−326.
(53) Jayaprakash, K.; Banerjee, U.; Sen, A. *Langmuir* **2016**, *32*, 2136−2143.
(54) Jayaprakash, K.; Banerjee, U.; Sen, A. *J. Colloid Interface Sci.* **2017**, *493*, 317−326.
(55) Tian, F.; Zhang, W.; Cai, L.; Li, S.; Hu, G.; Cong, Y.; Liu, C.; Li, T.; Sun, J. *Lab Chip* **2017**, *17*, 3078.
(56) Yuan, D.; Tan, S. H.; Sluyter, R.; Zhao, Q.; Yan, S.; Nguyen, N.-T.; Guo, J.; Zhang, J.; Li, W. *Anal. Chem.* **2017**, *89*, 9574.
(57) D'Avino, G.; Hulsen, M.; Maffettone, P. *Comput. Fluids* **2013**, *86*, 45−55.
(58) Macosko, E. Z.; et al. *Cell* **2015**, *161*, 1202−1214.

DOI: 10.1021/acs.analchem.7b02450
Anal. Chem. 2017, 89, 13146−13159